Pergamon

Geochimica et Cosmochimica Acta, Vol. 68, No. 2, pp. 345–360, 2004

0016-7037/04 $30.00 + .00

doi:10.1016/S0016-7037(03)00419-8

Length scales of mantle heterogeneities and their relationship to ocean island basalt geochemistry

TETSU KOGISO,[1,2,*] MARC M. HIRSCHMANN,[1] and PETER W. REINERS[3]

[1]Department of Geology and Geophysics, University of Minnesota, Minneapolis, MN 55455, USA
[2]Institute for Frontier Research on Earth Evolution, Japan Marine Science and Technology Center, Yokosuka, Kanagawa 237-0061, Japan
[3]Department of Geology and Geophysics, Yale University, New Haven, CT 06520, USA

(*Received December* 17, 2002; *accepted in revised form June* 9, 2003)

Abstract—The upper mantle is widely considered to be heterogeneous, possibly comprising a "marble-cake" mixture of heterogeneous domains in a relatively well-mixed matrix. The extent to which such domains are capable of producing and expelling melts with characteristic geochemical signatures upon partial melting, rather than equilibrating diffusively with surrounding peridotite, is a critical question for the origin of ocean island basalts (OIB) and mantle heterogeneity, but is poorly constrained. Central to this problem is the characteristic length scale of heterogeneous domains. If radiogenic osmium signatures in OIB are derived from discrete domains, then sub-linear correlations between Os isotopes and other geochemical indices, suggesting melt-melt mixing, may be used to constrain the length scales of these domains. These constraints arise because partial melts of geochemically distinct domains must segregate from their sources without significant equilibration with surrounding peridotite. Segregation of partial melts from such domains in upwelling mantle is promoted by compaction of the domain mineral matrix, and must occur faster than diffusive equilibration between the domain and its surroundings. Our calculations show that the diffusive equilibration time depends on the ratios of partition and diffusion coefficients of the partial melt and surrounding peridotite. Comparison of time scales between diffusion and melt segregation shows that segregation is more rapid than diffusive equilibration for Os, Sr, Pb, and Nd isotopes if the body widths are greater than tens of centimeter to several meters, depending on the aspect ratio of the bodies, on the melt fraction at which melt becomes interconnected in the bodies, and on the diffusivity in the solid. However, because Fe-Mg exchange occurs significantly more rapidly than equilibration of these isotopes under solid-state and partially molten conditions, it is possible that some domains can produce melts with Fe/Mg ratios reflecting that of the surrounding mantle but retaining isotopic signatures of heterogeneous domains. Although more refined estimates on the rates of, and controls on, Os mobility are needed, our preliminary analysis shows that heterogeneous domains large enough to remain compositionally distinct in the mantle (as solids) for $\sim 10^9$ yr in a marble-cake mantle, can produce and expel partial melts faster than they equilibrate with surrounding peridotite.

1. INTRODUCTION

Mantle heterogeneity is well established from geochemical and geophysical studies, but the distribution, scale, magnitude, and origin of mantle heterogeneities remain controversial (Brandon et al., 1998; Kamber and Collerson, 1999; Norman and Garcia, 1999; Rudnick et al., 2000). An essential constraint on the origin and consequences of mantle heterogeneity is the scale of heterogeneous domains. Geophysical observations indicate that heterogeneity may be present on the scale of 10^4 m or greater, (e.g., Ishii and Tromp, 1999; Kaneshima and Helffrich, 1999; Zhao, 2001) but do not currently allow resolution of finer scale features. Regional geochemical variations of OIB, however, require mantle heterogeneity on a 10^3-m scale (Gast et al., 1964; Zindler and Hart, 1986) and some geochemically-based models of basalt source regions call on heterogeneities ranging from decimeter-scale veins found in orogenic peridotite massifs (Allègre and Turcotte, 1986; Reisberg et al., 1991) (but see also Blichert-Toft et al., 1999) to kilometer-scale bodies of subducted oceanic crust (Hauri, 1996; Hanyu and Kaneoka, 1997). Presumably, mantle heterogeneities have a range of scales, but quantitative constraints on their size distributions in basalt source regions is important because their dimensions may strongly affect the dynamics of melting and the geochemistry of integrated melts. Knowledge of their sizes may also have implications for the possible origins and history of such domains.

Hofmann and Hart (1978) showed that centimeter-sized heterogeneities can remain compositionally distinct in the solid mantle for billions of years, but that partial melting might homogenize even much larger bodies ($\sim$20 m) over time scales as short as 10^5 to 10^6 yr. Consequently, they argued that small compositional heterogeneities can be maintained over the lifetime of the Earth, but are erased by diffusion in partially melting basalt source regions. In recent years, evidence for small-scale heterogeneities in basalt source regions has mounted, most notably from trace element and isotopic studies of melt inclusions in phenocrysts from basalts (Saal et al., 1998; Sobolev et al., 2000), and apparent isotopic discrepancies between oceanic basalts and their inferred abyssal peridotite sources (Salters and Dick, 2002). Partly in response to these lines of evidence, models invoking decimeter-scale mafic veins to explain features of basalt geochemistry have proliferated. At the same time, modern models for melt extraction and U-series isotopes of oceanic basalts both indicate that melt extraction time scales are 10^3 yr or less, rather than the 10^5 to 10^6 yr

* Author to whom correspondence should be addressed, at the Department of Earth and Planetary Sciences, Tokyo Institute of Technology, Tokyo 152-8551, Japan (kogisot@jamstec.go.jp).

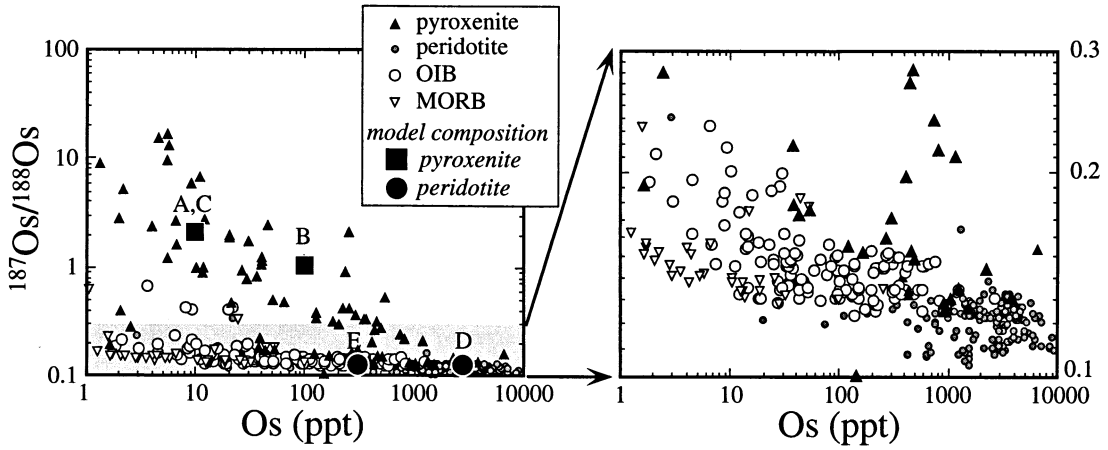

Fig. 1. Variations of Os isotopic ratios and concentrations in peridotite, pyroxenite, OIB and MORB. Large solid symbols are the model compositions for pyroxenite (A, B), pyroxenite partial melt (C), peridotite (D), and peridotite partial melt (E) used in the mixing calculations for Figure 2e. Data are from Reisberg et al. (1991), Carlson and Irving (1994), Pearson et al. (1995), Kumar et al. (1996), McBride et al. (1996), Roy-Barman et al. (1996), Esperanca et al. (1997), Olive et al. (1997), Becker (2000), Lassiter et al. (2000), Becker et al. (2001), Saal et al. (2001), and the Os-isotope database of Woods Hole Oceanographic Institution (http://www.whoi.edu/NobleMetals).

considered previously (McKenzie, 2000; Maclennan et al., 2002). However, with few exceptions (e.g., Phipps Morgan, 1999), there has been little attempt to reconcile these developments with the paradigm of Hofmann and Hart (1978).

Analysis of the role of small-scale heterogeneities on aggregate basalt compositions has the potential to constrain the physical dimensions of compositional source domains and mechanisms of melt transport. In partially molten regions, chemical heterogeneities can be partly or wholly destroyed by diffusive interactions with surrounding rock and melt (Hofmann and Hart, 1978). However, as detailed below, compositional variations in OIB apparently require that distinct melt compositions are extracted from heterogeneities before the geochemical identities of sources are destroyed by diffusion. Thus, the bodies must be sufficiently large such that melt segregation is rapid compared to diffusive equilibration with surrounding mantle, and in theory this places limits on the length scale of chemical heterogeneities in the melt source.

Many studies of OIB suites have noted near-linear correlations among geochemical parameters (isotopic ratios, trace element abundances or ratios) and concluded that these are best explained by mixing between melts, rather than mixing between source lithologies or between melts and solid reservoirs (Chen and Frey, 1985; Martin et al., 1994; Class and Goldstein, 1997; Kamber and Collerson, 1999, 2000; Phipps Morgan, 1999; Lassiter et al., 2000; Reiners, 2002). This is because mixing trends for ratios are strongly non-linear if the contributing components have strongly contrasting elemental concentrations. In many cases it is more reasonable to assume subequal concentrations of elements in distinct partial melts, rather than in the sources of those melts. If melt-melt mixing is common in OIB source regions, segregation of partial melts from their sources must be rapid relative to diffusive homogenization and so can be used to constrain the size distribution of the heterogeneous domains.

In this study, we consider the competing processes of diffusion and melt segregation which determine whether partial melts preserve the characteristics of their source. We focus on linear correlations of Os isotopes with other geochemical species in OIB suites, because the contrasts in Os concentrations and isotope ratios between peridotites and pyroxenites make the Os geochemistry of lavas highly sensitive to melt segregation processes.

2. CONSTRAINTS FROM OSMIUM ISOTOPES OF OIB

Key evidence for the possible presence and dimension of mafic lithologies in the source regions of OIB may come from Os isotopes. This is because widespread radiogenic Os isotopic ratios of OIB are not consistent with an origin solely from typical peridotitic sources, which are characterized by relatively unradiogenic Os. The radiogenic Os of OIB suggests participation of mafic lithologies (pyroxenite and eclogite), which have highly radiogenic Os (Fig. 1) (e.g., Hauri and Hart, 1993; Schiano et al., 1997; Lassiter et al., 2000). Importantly, most mafic lithologies likely to be present in the mantle, hereafter called pyroxenites (e.g., Hirschmann and Stolper, 1996), have much lower Os concentrations than peridotite (Fig. 1). In contrast, concentrations of incompatible trace elements, such as Sr, Nd and Pb, are generally higher in pyroxenite than peridotite (Hirschmann and Stolper, 1996, and references therein), indicating that interaction of pyroxenite or pyroxenite-derived melt with peridotite could easily obliterate the pyroxenite's radiogenic Os signature but may not affect significantly its signature in incompatible tracers.

In a number of prominent OIB case studies, Os isotopes correlate nearly linearly with other isotope ratios and trace element abundances (Figs. 2a–2d). Such trends are significant evidence favoring mixing of melts from distinct sources. Melts derived from varying proportions of solid-solid mixing (i.e., solid mixtures of peridotite and pyroxenite) will form strongly curved mixing trajectories (Fig. 2e) because of the large differences in Os-incompatible element ratios between peridotite and pyroxenite (Hauri and Hart, 1993; Class and Goldstein,

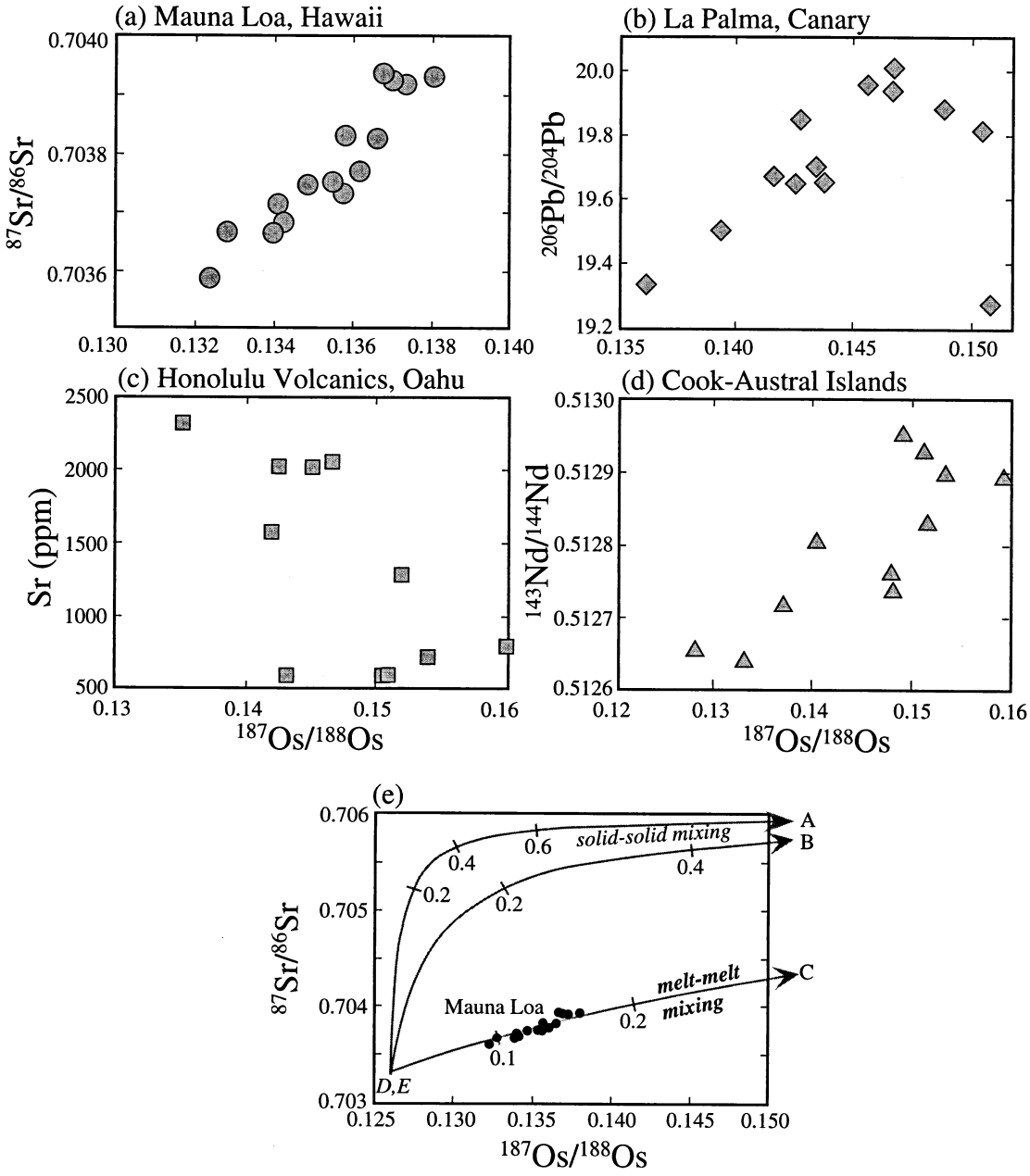

Fig. 2. (a) to (d) Examples of the linear correlations between Os isotopes and other isotopic ratios and trace element concentrations observed in OIB suites. (a) Tholeiitic lavas from Mauna Loa, Hawaii Island (Hauri and Kurz, 1997). (b) Basanites from La Palma Island, Canary (Marcantonio et al., 1995). (c) Alkali olivine basalts and nephelinites from eight vents of Honolulu Volcanics, Oahu Island, Hawaii (Lassiter et al., 2000). (d) Alkali basalts and basanites from nine islands of Cook-Austral chain (Schiano et al., 2001). (e) Comparison of Mauna Loa Os-Sr isotope array (from panel a) with models of solid-solid and melt-melt mixing from a peridotite-pyroxenite source. Two representative pyroxenite compositions, A and B, are employed (see Fig. 1 for comparison to natural compositions). Mixing trends are calculated between pyroxenite solid (A, B) and peridotite solid (D) and between pyroxenite partial melt (C) and peridotite partial melt (E). Compositions of model end members are A: Os = 10 ppt, $^{187}Os/^{188}Os$ = 2.0, Sr = 100 ppm, $^{87}Sr/^{86}Sr$ = 0.7060; B: Os = 100 ppt, $^{187}Os/^{188}Os$ = 1.0, Sr = 100 ppm, $^{87}Sr/^{86}Sr$ = 0.7060; C: Os = 10 ppt, $^{187}Os/^{188}Os$ = 2.0, Sr = 300 ppm, $^{87}Sr/^{86}Sr$ = 0.7060; D: Os = 3000 ppt, $^{187}Os/^{188}Os$ = 0.126, Sr = 10 ppm, $^{87}Sr/^{86}Sr$ = 0.7033; E: Os = 300 ppt, $^{187}Os/^{188}Os$ = 0.126, Sr = 200 ppm, $^{87}Sr/^{86}Sr$ = 0.7033. Tick marks represent proportion of pyroxenite (top two curves) or pyroxenite partial melt (bottom curve) present in mixture. We assume that preferential melting enhances the proportion of pyroxenite partial melt by a factor of 3 relative to the proportion of pyroxenite in the source (Hirschmann and Stolper, 1996; Pertermann and Hirschmann, 2003). Mixing of peridotite and pyroxenite solids produces strongly curved arrays and requires substantial proportions of pyroxenite (60% for A, 25% for B) to attain $^{187}Os/^{188}Os$ comparable to the most radiogenic Mauna Loa lavas. In contrast, mixing of partial melts of peridotite and pyroxenite produces a near linear array and requires $<$ 5% pyroxenite in the source ($<$15% pyroxenite partial melt) to reproduce array.

1997; Becker, 2000). For similar reasons, melt-solid reaction between pyroxenite melt and peridotite solid would produce curved trends unlike the examples in Figures 2a to 2d. Even if these linear trends could be produced by melting of solid sources containing uniformly and thoroughly mixed peridotite and pyroxenite in different proportions, the most radiogenic OIB lavas would require a source with ~20 to 95% of the pyroxenite, more than is geochemically or geodynamically reasonable (e.g., Brandon et al., 1998; Walker et al., 1999; Becker, 2000). Similar proportions result from reaction between pyroxenite partial melt and solid peridotite (Class and Goldstein, 1997; Hauri, 1997). Thus, if pyroxenite is the source of radiogenic Os in OIB, it cannot mix or exchange with significant amounts of solid peridotite.

Mixing between partial melts of pyroxenite and partial melts of peridotite could occur in the mantle or crust and could explain near-linear trends between $^{187}Os/^{188}Os$ and incompatible tracers. Os concentrations in partial melts of peridotite should be much less than in the bulk rock, so long as sulfide remains in the residue (Hart and Ravizza, 1996; Blusztajn et al., 2000; Burton et al., 2000). In contrast, partial melts of pyroxenite should have Os concentrations similar to their source, as relatively high degrees of melting and exhaustion of residual sulfides are expected. Thus, Os concentration contrasts between partial melts from the two lithologies may be much smaller than between the two solids. On the other hand, concentrations of incompatible elements in pyroxenite are higher than in peridotite, and higher degrees of melting of pyroxenite relative to peridotite result in smaller contrasts incompatible element concentrations between the two partial melts. As a result, the contrast in Os-incompatible element ratios between pyroxenite-derived melt and peridotite-derived melt will likely be sufficiently small such that mixing of the two melts forms near-linear trends between $^{187}Os/^{188}Os$ and incompatible tracers such as $^{87}Sr/^{86}Sr$ (Fig. 2e). Furthermore, only modest proportions of pyroxenite would be required to span the range of $^{187}Os/^{188}Os$ observed (Fig. 2e). Because preferential melting of pyroxenite relative to peridotite (Hirschmann and Stolper, 1996; Pertermann and Hirschmann, 2003) also decreases the proportion of pyroxenite source rock required, the most radiogenic Os and Sr isotopic ratios found in Mauna Loa lavas require only ~5% pyroxenite in the source in the model shown in Figure 2e.

It is important to recognize that many basalts are Os-poor, and so are potentially contaminated by radiogenic Os by crustal contamination or sea-water alteration (e.g., Reisberg et al., 1993; Marcantonio et al., 1995). However, as shown in Figure 1, radiogenic $^{187}Os/^{188}Os$ is also a feature of Os-rich (100–1000 ppt Os) OIB, which are less likely to be affected by shallow contamination (Hauri et al., 1996; Brandon et al., 1999; Walker et al., 1999; Bennet et al., 2000). Further, processes that could impart radiogenic Os signatures to relatively primitive magmas should be detectable from other geochemical parameters (e.g., Reisberg et al., 1993; Widom et al., 1999; Lassiter et al., 2000; Carlson and Nowell, 2001). Evidence for a deep origin for radiogenic Os in mantle-derived magmas is also provided by radiogenic $^{187}Os/^{188}Os$ in mantle dunites, which is believed to result from extensive reaction between peridotite with radiogenic melts (Burton et al., 2000; Becker et al., 2001; Büchl et al., 2002). Thus, radiogenic Os in OIB (Fig. 1) requires a source in the mantle.

An alternative explanation for radiogenic Os in OIB is that it represents small contributions of the outer core to deep-sourced mantle plumes (Walker et al., 1995). Brandon et al. (1998, 1999) noted that recycled crust might explain correlated enrichments of $^{186}Os/^{188}Os$ and $^{187}Os/^{188}Os$ observed in Hawaii, but preferred the core as a source because the proportion of recycled crust required to account for both high $^{186}Os/^{188}Os$ and $^{187}Os/^{188}Os$ seemed to them untenable. Similar objections to recycled sources of radiogenic $^{187}Os/^{188}Os$ in the Gorgona plume have been raised by Walker (1999). However, only modest proportions of a recycled component are needed if melt-melt mixing is responsible for $^{187}Os/^{188}Os$ variations in OIB (Fig. 2). Also, Brandon et al. (1999) noted that the data then available did not include potential sources of recycled materials with Pt/Re ratios large enough to explain the steep $^{186}Os/^{188}Os$ vs. $^{187}Os/^{188}Os$ trend of Hawaiian lavas. However, recently published studies reveal that a range of lithologies, including harzburgite from Troodos Ophiolite (Büchl et al., 2002), mantle xenoliths from the Sierra Nevada (Lee, 2002) and metalliferous sediments (Ravizza et al., 2001) have Pt/Re ratios at least as high as that required for the high $^{186}Os/^{187}Os$ component in Hawaii. Finally, it seems unlikely that a core component can explain near-linear correlations between $^{187}Os/^{188}Os$ and incompatible tracers (Fig. 2), and so a recycled component seems a better explanation for radiogenic $^{186}Os/^{188}Os$ and $^{187}Os/^{188}Os$ in Hawaii.

In summary, significant circumstantial evidence suggests that radiogenic $^{187}Os/^{188}Os$ in OIB (Fig. 1) derives from pyroxenite in the OIB source. If this is so, then near-linear correlations between Os isotopes and incompatible tracers in OIB (Fig. 2) are best explained by mixing between partial melts derived from pyroxenite and peridotite. In the next section, we summarize the conditions under which mixing between melts from distinct sources is possible, and consider how it can be used to constrain the length scales of pyroxenite domains in OIB sources.

3. PERIDOTITE-PYROXENITE INTERACTIONS IN THE MANTLE

Mixing between melts derived from pyroxenite and peridotite is only interpretable if each melt preserves the geochemical character of its source until mixing occurs. As illustrated in Figure 3, this requires that (I) before melting, solid pyroxenite must not equilibrate with peridotite, (II) melt must be separated from the pyroxenite source more rapidly than diffusive equilibration between partially molten pyroxenite and surrounding peridotite, and (III) the separated melt must retain the characteristics of its source during transport to the locus of mixing. Here we outline the approaches we take to address these problems in this study. *A critical aspect of our analysis is that we recognize initial separation of melt from its source (II) and transport of melt through overlying mantle (III) as distinct processes.* It is the former that provides the most direct constraints on the length scale of source heterogeneities.

The chief parameter influencing process (I) is the dimension of pyroxenite needed to maintain geochemical isolation during extended (10^8–10^9 yr) residence in the mantle. A generalized

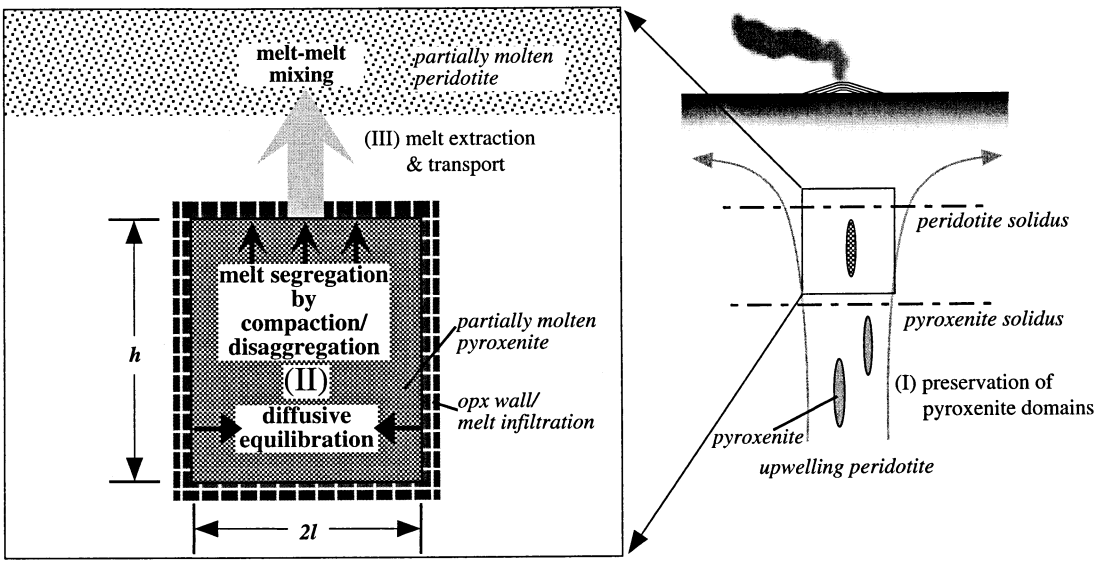

Fig. 3. Schematic illustration of partial melting processes of heterogeneous mantle. Mixing of pyroxenite partial melt with peridotite partial melt, inferred from Os isotopes (Fig. 2e), requires the following: (1) before melting, the geochemical character of pyroxenite bodies within upwelling peridotite is preserved. (2) Once partial melting of pyroxenite begins, melts segregate from pyroxenite sources faster than they equilibrate diffusively with peridotite. (3) Once segregated from their pyroxenite source, partial melts traverse peridotite without extensive exchange with large volumes of peridotite. Pyroxenite partial melts mix with peridotite partial melts either in magma chambers, melt-filled channels or in conduits that experience high melt/rock ratios.

version of this problem was evaluated by Hofmann and Hart (1978). Perhaps most important for the viability of mantle heterogeneities in basalt petrogenesis is whether bodies that survive extended solid-state residence in the mantle (I) are large enough to allow rapid separation of geochemically distinct melt (II).

The next topic we consider is production of geochemically distinct melts from pyroxenite sources. In or near the source region, this is a question of competition between melt segregation and wall-rock equilibration time scales (II), and has received little quantitative attention previously. Pyroxenite domains in upwelling mantle start melting at greater depths than the surrounding peridotite (Fig. 3) (Yasuda et al., 1994; Pertermann and Hirschmann, 2003). As we will show, for partially molten pyroxenite bodies, the relative time scales of melt segregation and equilibration with solid peridotite wall-rock depend on the length scale of the domains. Thus, if geochemical observations (e.g., Os isotope correlations) require segregation of melts from pyroxenite residues before their character is destroyed by diffusive equilibration with surrounding peridotite, the minimum length scales of heterogeneous domains are constrained.

Preservation of source signatures during melt extraction and transport through the mantle (III) is one of the critical factors influencing the geochemistry of mantle-derived magmas. Consequently, it has been addressed in numerous studies (e.g., Spiegelman and Kenyon, 1992; Iwamori, 1993; Hauri, 1997; Kelemen et al., 1997). Owing to the large Os partition coefficient between peridotite residual mineralogies and silicate melt, grain-scale porous flow through peridotite should destroy radiogenic Os signatures of percolating melts after not more than 200 m transport (Hauri and Kurz, 1997). Thus, OIB with radiogenic Os require that magmas migrate from radiogenic Os sources (such as pyroxenite) to the surface without extensive reaction with typical peridotite. Such melts must ascend without extensive interaction (e.g., via fractures) or via restricted porous channels at high melt/rock ratio, as evidenced perhaps by radiogenic Os in dunite conduits (Burton et al., 2000; Becker et al., 2001; Büchl et al., 2002). This inference is consistent with trace element systematics of oceanic basalts, which do not show significant effects of chromatographic effects of melt-rock interactions (Hauri and Kurz, 1997; Reiners, 1998). The main aim of this paper is to constrain length scales of pyroxenite domains by focusing on process (II), so we do not address the issue of transport in detail. But in the "Discussion" we consider how melting and segregation from heterogeneities may aid rapid transport of enriched melts through the overlying mantle.

3.1. Subsolidus Interactions

Pyroxenites may originate by many different processes (Hirschmann and Stolper, 1996), but subducted oceanic crust is the volumetrically dominant potential source. Before entering the source regions of modern basalts, recycled oceanic crust likely undergoes a complex chemical and physical evolution. In addition to effects during subduction (e.g., McCulloch and Gamble, 1991; Kogiso et al., 1997), significant changes may occur during the subsequent interval before recirculation to basalt source regions. Associated processes are difficult to quantify because recycled components may reside in one or several different environments, including the upper mantle, transition zone, lower mantle, and core-mantle boundary.

Sections of subducted crust originate as bodies several km

thick, but convective stretching reduces their widths exponentially with time (Allègre and Turcotte, 1986; Kellogg and Turcotte, 1990). Simple two-dimensional parameterization of convective thinning suggests that subducted crust is stretched to subcentimeter widths in < 1 billion years (Kellogg and Turcotte, 1990). Consideration of convection in three dimensions (van Keken and Zhong, 1999) and the likely enhanced viscosity of recycled crust in the transition zone and lower mantle (Merveilleux du Vignaux and Fleitout, 2001) suggests much longer stretching times. In the absence of melting, destruction of heterogeneities occurs via diffusion, but melt-absent diffusive homogenization is effective only over a few tens of centimeters on billion-year time scales (Hofmann and Hart, 1978).

Subducted oceanic crust transforms to a silica-saturated pyroxenite, which cannot be in equilibrium with olivine or its polymorphs in the upper mantle or with ferropericlase in the lower mantle. Consequently, reaction skarns rich in orthopyroxene (opx) (or its high-pressure equivalent) should form at peridotite/pyroxenite interfaces. Growth of a medial opx layer between olivine and a silica phase is controlled by interdiffusion of Mg, Fe and Si along opx grain boundaries (Fisler et al., 1997; Yund, 1997; Milke et al., 2001). The experiments of Fisler et al. (1997), when adjusted to typical (1 mm) mantle grain sizes, predict growth of a 40 to 90 cm wide opx layer between silica and forsterite over 2 billion years at 1350 to 1450°C, respectively. However, the opx-rich layer likely to grow between peridotite and pyroxenite layers should be thinner. This is because the actual mode of free silica in pyroxenite is no more than a few percent, so the flux of silica to the growing layer would be mediated by diffusion within other phases and/or grain boundaries. Also, reaction layer growth is likely retarded in the lower mantle, owing to very slow Si diffusion in Mg-perovskite (Yamazaki et al., 2000). Convective stretching would reduce the thickness of both the pyroxenite and the opx-rich layer as the latter grows, and so the resulting spatial scales will depend on the relative rates of these processes. Medial opx growth may produce the websterite bands common in orogenic lherzolites (e.g., Bodinier et al., 1987; Kumar et al., 1996) and olivine websterite xenoliths such as the well-known HK-66 nodule from Salt Lake Crater, Hawaii (Kushiro et al., 1968; I. Kushiro, personal communication 2001).

3.2. Interactions in Basalt Source Regions

In upwelling mantle, pyroxenite domains begin to partially melt surrounded by unmelted peridotite (Yasuda et al., 1994; Pertermann and Hirschmann, 2003), and so the mechanisms and time scales of melt segregation may be distinct from those prevailing in large columns of partially molten peridotite. After the onset of partial melting in pyroxenite, equilibration of the melt with surrounding mantle can be promoted by diffusion of chemical species through an interconnected network of melt-filled tubules. At the same time, separation of melt from residual pyroxenite can occur either by infiltration into surrounding peridotite (Daines and Kohlstedt, 1993) or by an internal separation process yielding melt-rich and crystal-rich subregions in the former solid pyroxenite body. Internal segregation could occur by compaction of the solid matrix (McKenzie, 1984) or, if infiltration and compaction are slow relative to melting, disaggregation and crystal settling of the pyroxenite matrix at high melt fraction.

Infiltration of partial melts into surrounding peridotite can only occur if surrounding peridotite has finite permeability, which requires survival of liquid percolating into grain boundaries of peridotite. Crystallization of such liquids upon contact with peridotite would eliminate permeability and prevent further infiltration (Daines and Kohlstedt, 1993). If pyroxenite begins to melt at temperatures well below the peridotite solidus, the composition of partial melt will determine whether the reaction between melt and peridotite promotes or impedes infiltration. Partial melts of MORB-like pyroxenite are silica-saturated and will crystallize upon contact with peridotite, resulting in formation of opx-rich bands at peridotite/pyroxenite interfaces (Yaxley and Green, 1998; Takahashi and Nakajima, 2002). Preexisting opx-rich bands formed below the solidus (see section 3.1) may simply grow. Regardless, such bands impede further infiltration, so reaction between melt in the interior of the heterogeneity and the surrounding peridotite proceeds only by diffusion across them. Competition between this diffusion and segregation by compaction or disaggregation determines whether partial melts retain or lose the signature of their source. If partial melt from a pyroxenite body is silica-undersaturated (Kogiso and Hirschmann, 2001; Hirschmann et al., 2003), orthopyroxene may dissolve rather than precipitate at the pyroxenite/peridotite boundary (Bulatov et al., 2002) and reactive infiltration of melt into the peridotite might proceed (e.g., Daines and Kohlstedt, 1993; Kelemen et al., 1997; Lundstrom, 2000).

If infiltration of partial melt into surrounding peridotite is inhibited, extensive melting, possibly aided by compaction, could produce melt-rich regions of pyroxenite. These will be mechanically weak, and the strength contrast relative to solid peridotite may nucleate mechanical instabilities, even for modest accumulations of melt (Stevenson, 1989). Such instabilities would presumably cause periodic expulsion of melt into veins or channels. The occurrence and time-dependence of such events depend on a range of factors (stresses, mechanical properties) that are beyond the scope of the present analysis. We assume that such mechanisms would be rapid relative to diffusional time scales and that formation of melt-rich regions is a condition sufficient to yield segregation of compositionally distinct pyroxenite-derived melts.

3.3. Summary

Mantle pyroxenite domains interact continuously with enclosing peridotite, and though convective stretching reduces their size, pyroxenite bodies remain as discrete solid-state entities until they are destroyed by diffusive exchange at pyroxenite/peridotite margins. Once pyroxenites begin to partially melt, diffusive interactions accelerate, thereby aiding in their destruction. However, partial melts may also segregate from their source rapidly, and so the geochemical character of melts segregating from such heterogeneities depends on the relative rates of melt-aided diffusion, melt segregation, and length scale of the heterogeneity.

4. QUANTITATIVE MODELS OF DIFFUSION AND MELT SEGREGATION

Here we analyze the relationship between length scales of heterogeneities and time scales of diffusive equilibration and melt segregation within a partially molten pyroxenite body surrounded by solid peridotite (process II from section 3 and Figure 3) based on quantitative models. The time scale of diffusive equilibration is calculated for one-dimensional diffusion between a small partially molten pyroxenite heterogeneity and surrounding solid peridotite. We estimate the time scale of melt segregation from compaction of the partially molten body. We then compare the two time scales and constrain the size of body that will allow melt to segregate before diffusive equilibration with surrounding peridotite.

4.1. Diffusive Equilibration Within Two-Layer Composite Media

We consider one-dimensional diffusion in a system consisting of a partially molten pyroxenite region with half width l, embedded in an infinite reservoir of peridotite (Fig. 3). This represents the scenario envisioned for the deepest part of a heterogeneous mantle melting column (e.g., Hirschmann and Stolper, 1996), in which pyroxenite domains cross their solidi before, and begin melting at greater depths than, the peridotite matrix (Fig. 3). For simplicity, we assume no flux between pyroxenite partial melt and residual minerals. The governing equations are

$$\frac{\partial(\phi c_{xm})}{\partial t} = D_{xm}\frac{\partial^2(\phi c_{xm})}{\partial x^2} + c_{xs}\frac{\partial \phi}{\partial t} \qquad (-l < x < l) \tag{1}$$

$$\frac{\partial[(1-\phi)c_{xs}]}{\partial t} = D_{xs}\frac{\partial^2[(1-\phi)c_{xs}]}{\partial x^2} - c_{xs}\frac{\partial \phi}{\partial t} \qquad (-l < x < l) \tag{2}$$

$$\frac{\partial c_{pd}}{\partial t} = D_{pd}\frac{\partial^2 c_{pd}}{\partial x^2} \qquad (x < -l, \text{ and } x > l) \tag{3}$$

where t is time, x is distance from the center of the partial molten region, c_{xm}, c_{xs} and c_{pd} are the concentrations of the diffusing species, D_{xm}, D_{xs}, and D_{pd} are diffusion coefficients in the pyroxenite partial melt, pyroxenite residual solid and surrounding solid peridotite, respectively, and ϕ is the porosity (= melt fraction) of the pyroxenite. Because this system is symmetric about $x = 0$, we hereafter consider only the region of $x \geq 0$.

We approximate the fractions of cross-sectional area of the pyroxenite melt and solid perpendicular to the boundary between the pyroxenite and peridotite by their volume fractions. We also assume equilibrium between c_{xm} and c_{pd} at the pyroxenite-peridotite boundary and no accumulation of diffusing component at the boundary. Thus, the boundary conditions are

$$\phi D_{xm}\frac{\partial c_{xm}}{\partial x} + (1-\phi) D_{xs}\frac{\partial c_{xs}}{\partial x} = D_{pd}\frac{\partial c_{pd}}{\partial x} \qquad (x = l) \tag{4}$$

$$\frac{c_{pd}}{c_{xm}} = k \qquad (x = l) \tag{5}$$

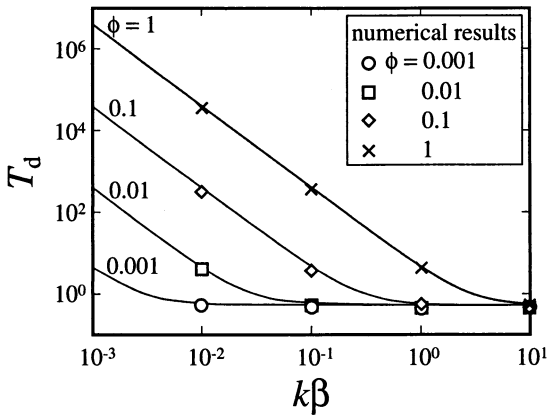

Fig. 4. Dimensionless diffusion time (T_d) plotted against $k\beta$ ($k = c_{pd}/c_{xm}$, $\beta = [D_{pd}/D_{xm}]^{0.5}$). Symbols are numerical calculations for various values of ϕ. Solid curves are fits of numerical results given by Eqn. 7. When ϕ is small or $k\beta$ is large, the diffusion time is independent of $k\beta$, meaning that the rate-limiting process is diffusion in the pyroxenite body (see text).

$$\frac{\partial c_{xm}}{\partial x} = \frac{\partial c_{xs}}{\partial x} = 0 \qquad (x = 0) \tag{6}$$

where k is the partition coefficient of the diffusing species between solid peridotite and pyroxenite partial melt.

Here we calculate the simplest case in which ϕ is constant and the diffusing species is completely incompatible to the pyroxenite solid ($c_{xs} = 0$). The latter assumption has the effect of minimizing calculated diffusion times (i.e., in the real system, the finite pyroxenite/melt partition coefficient would lead to slower diffusive equilibration, and smaller minimum pyroxenite domains). The equations are made dimensionless ($T = tD_{xm}/l^2$, $X = x/l$) and then solved numerically using the Crank-Nicolson method (Crank, 1956). We calculate the dimensionless diffusion time T_d, which is that required for the diffusing species to reach $e/(e + 1)$ (~73%) of its equilibrium concentration (i.e., that attained at $T = \infty$), at which point it has lost its distinctive chemical signature. T_d is a function of melt fraction and the relative concentrations and diffusivities of the diffusing species, which can be parameterized as $k\beta$, where $\beta = (D_{pd}/D_{xm})^{0.5}$. Calculated values of T_d are shown as a function of $k\beta$ in Figure 4. The trends in Figure 4 show that T_d can be parameterized as

$$T_d = \frac{4\phi^2}{(k\beta)^2} + \frac{1}{2} \tag{7}$$

As shown in Figure 4, if $k\beta$ is $> \sim 10$, T_d is independent of $k\beta$ and ϕ, and Eqn. 7 reduces to $T_d = 1/2$. This leads to a diffusion time in the real dimension, t_d, equal to $l^2/(2D_{xm})$. Thus, for large values of $k\beta$, homogenization of pyroxenite depends on diffusion within the pyroxenite body according to normal $\sqrt{D_{xm}t}$ relations, but for smaller values $k\beta$, it is rate-controlled by diffusion through the surrounding peridotite.

4.2. Melt Segregation by Compaction

We evaluate the time scale for melt segregation induced by compaction of the matrix of a partially molten body using the

model of McKenzie (1984, 1985). For a partially molten body with height h, the compaction time t_c, which is that required to reduce by a factor of e the mass of melt in the partially molten region, is described by

$$t_c = \left(\frac{h}{\delta_c} + \frac{\delta_c}{h}\right)\tau_0 \tag{8}$$

where the compaction length, δ_c, is given by

$$\delta_c = \sqrt{\frac{\left(\zeta + \frac{4}{3}\eta\right)k_\phi}{\mu}} \tag{9}$$

the reference time, τ_0, is

$$\tau_0 = \frac{\delta_c}{w_0(1-\phi)} \tag{10}$$

and the fluid velocity, w_0, is

$$w_0 = \frac{k_\phi(1-\phi)(\rho_s-\rho_m)g}{\mu\phi} \tag{11}$$

Here, ζ and η are the effective bulk and shear viscosities of the matrix, ρ_s and ρ_m are the densities of the matrix and melt, g is gravitational acceleration, μ is the shear viscosity of the melt, and ϕ is the porosity. k_ϕ is the permeability of the matrix, commonly defined as

$$k_\phi = \frac{a^2\phi^n}{b} \tag{12}$$

where a is the grain size, b is a geometrical constant, and n is a constant between 1 and 3 (Riley et al., 1990; Daines and Kohlstedt, 1993). This model is applicable only for the case of constant ϕ. We consider the case for which the height of the body is larger than its width; i.e., $h \geq 2l$. For bodies with widths greater than their height, vertical diffusive paths are shorter than horizontal paths and the length scale for diffusive equilibration, l, is vertical and therefore equal to $h/2$.

4.3. Competition Between Diffusive Equilibration and Melt Segregation

Separation of melt from a pyroxenite source without significant equilibration with surrounding peridotite depends on the relative time scales of diffusion and melt segregation in pyroxenite domains, which in turn depend on pyroxenite domain size and other characteristics. Here we examine the critical parameters affecting diffusion and melt segregation to see how they affect the body size for which homogenization is more rapid than melt separation. Note that this part of the process requires only that melt-rich areas form in the pyroxenite (process II from section 3, above); i.e., no assumptions are required about transport after melt leaves its source.

The models for diffusion and compaction developed here are applicable only for the case of constant ϕ, and are restricted to cases in which the melting rate is slow relative to compaction, such that the porosity remains near the threshold for melt interconnection (see below). If compaction is slow relative to the melting rate, the local melt fraction can become large and the matrix grains will lose contact with one another, allowing disaggregation; i.e., crystal settling and consequent separation of partial melt (e.g., Marsh, 1981). In section 5.1 below, we evaluate the conditions under which disaggregation will occur more rapidly than compaction. For those cases where disaggregation is more rapid than compaction, survival of distinct chemical composition of partial melts from a heterogeneity depends on the competition between diffusion and disaggregation. Because our diffusion parameterization does not account explicitly for the effects of changing porosity, we do not model this competition in detail. However, for a reasonable range of values of $k\beta$, the diffusion time T_d for the variable porosity case will be similar to or longer than for the case where critical porosity is maintained by compaction, as T_d increases with porosity (Eqn. 7). Therefore, if the melting rate exceeds compaction, diffusive equilibration is either little-affected or inhibited, and the size of the body that allows melt to escape before homogenization with surrounding peridotite is unaffected or reduced.

4.3.1. Threshold Porosity for Melt Interconnection

As is clear from the above equations and Figure 4, porosity (ϕ) is the only parameter common to both diffusion and compaction time scales, and plays a key role in each. Once melt pockets in the partially molten body are interconnected along grain edges, extensive diffusive interaction with the surrounding peridotite and melt segregation by compaction may proceed.

Interconnection of melt in a partially molten body is expected at any porosity if the dihedral angle is $< 60°$, and is achieved for melt fractions equal to a few percent when it exceeds 60° by small amounts (von Bargen and Waff, 1986). The dihedral angle for clinopyroxene-melt textures is not well-known, but could exceed 60° (Toramaru and Fujii, 1986; Daines and Kohlstedt, 1993). We therefore examine end-member values for ϕ of 0.001 and 0.05.

4.3.2. Chief Parameters Affecting Diffusive Equilibration

Aside from porosity, the most important variables influencing diffusion are k and β ($= [D_{pd}/D_{xm}]^{0.5}$), except when the product $k\beta$ is large (>10), whereupon T_d becomes insensitive to $k\beta$ (Eqn. 7 and Fig. 4). Although partition coefficients and diffusivities are poorly known for Os, plausible ranges can be estimated, within which qualitatively similar conclusions result. Because linear correlations of Os isotopes with incompatible tracers in OIB (Fig. 2) suggest that variations in incompatible tracers also originate from mixing between from pyroxenite- and peridotite-derived liquids, k and β for Sr, Nd and Pb are also useful for the present analysis.

Estimated values of k, β and diffusivities and their sources are listed in Table 1. For incompatible elements (Sr, Nd and Pb), values of k are approximated as bulk partition coefficients between peridotite and basaltic melt with the assumptions that these elements in peridotite are partitioned only into clinopyroxene and that the mode of clinopyroxene in peridotite is 0.15. We estimate a value of k for Os of 30 to 300, based on typical ratios between pyroxenites and peridotites (Fig. 1). For diffu-

Table 1. Estimated parameters for diffusion between partially molten pyroxenite and solid peridotite.

Element	Principal host	log $D_{olivine}$[a]	log K[b]	log D_{pd}[c]	log D_{xm}[d]	log k[e]	log β
Os	Sulfide	–16.5 to –16.4	4 to 5	–21.5 to –20.4	–11.0 to –10.7	1.5 to 2.5	–5.4 to –4.7
Sr	cpx	–16.7	3.4	–20.1	–10.6	–1.8	–4.8
Nd	cpx	–22.0	3.3	–25.3	–10.9	–1.5	–7.2
Pb	cpx	–16.6	1.5	–18.1	–10.6	–3.0	–3.8
Fe-Mg	ol, cpx	–14.3[f]	0	–14.3	–10.5[g]	–0.5	–1.9

[a] Diffusion coefficient in olivine calculated using the model of Van Orman et al. (2001). Parameters used in the model are listed in Table 2.
[b] Partition coefficient between host mineral and olivine. Data source; sulfide-olivine: Hart and Ravizza (1996), Burton et al. (1999); olivine-melt: McKay (1986), Beattie (1993, 1994), Roeder and Emslie (1970); clinopyroxene (cpx)-melt: Beattie (1993), Hart and Dunn (1993), Hauri et al. (1994), Putirka (1999).
[c] = log ($D_{olivine}/K$).
[d] Calculated using the model of Hofmann (1980).
[e] The values for Os are estimated from typical ratios between pyroxenites and peridotites (Fig. 1), and those for Sr, Nd, and Pb are calculated assuming that the mode of clinopyroxene in peridotite is 0.15. Data sources are as for K.
[f] Jurewicz and Watson (1988).
[g] Kress and Ghiorso (1995).

sion in pyroxenite melt (D_{xm}), we apply the empirical relationship based on ionic charge and radius from Hofmann (1980).

Diffusion in peridotite requires transmission through the volumetrically dominant phase, olivine, even though most of the incompatible elements of interest (Sr, Nd, Pb) are concentrated in other silicates and most Os resides in sulfide or alloy (Hart and Ravizza, 1996; Burton et al., 1999, 2000). This results in reduced flux through the bulk peridotite and an effective diffusion coefficient of approximately $D_{pd} = D_{olivine}/K$, where K is the partition coefficient between the chief host mineral and olivine. Volume diffusion coefficients of all elements in olivine $D_{olivine}$ are estimated using the elastic model of Van Orman et al. (2001) (Table 2). Estimated values of K for incompatible elements are taken from partition coefficients of olivine- and clinopyroxene-melt pairs (Table 1) and for Os is from differences in concentration between sulfides and olivine in peridotite (Hart and Ravizza, 1996; Burton et al., 1999).

The values of D_{pd} estimated in Table 1 may be minima if there are mechanisms of rapid transport additional to lattice diffusion, such as grain boundary diffusion or through a grain-boundary molten sulfide phase. Grain boundary diffusion is generally thought to be inefficient relative to volume diffusion

Table 2. Parameters used to estimate diffusivity in olivine and clinopyroxene.

$$\ln D_z = \ln D_{z_{ref}}^{\delta=0} + b\left(1-\frac{z}{z_{ref}}\right) - 2b\left(\frac{z}{z_{ref}}\right)\left[\delta\left(1-\frac{1}{\sqrt{2}}\right)^{-1} - \delta^2\left(1-\frac{1}{\sqrt{2}}\right)^{-2}\right]$$

Lattice diffusion in olivine estimated from Eqn. 11 of van Orman et al. (2001), where b is defined as Eqn. 10 of Van Orman et al. (2001):

$$b = \frac{E_m^o}{R}\left[\frac{\partial(\mu/\mu_0)}{\partial T} + \frac{1}{T}\right] \text{ and } \delta = (r - r_{site})/r_0$$

Parameters at 1300°C are as follows:

Parameter	Olivine	Clinopyroxene[a]	Description
$\ln D_{z_{ref}}^{\delta=0}$	–32.9[b]	–45.8	Hypothetical D for reference ion with "ideal" radius
E_m^o	250[c]	330[g]	Activation enthalpy (kJ)
z_{ref}	2+	3+	Reference charge
$\partial(\mu/\mu_0)/\partial T$	–1.57[d]	–1.3[g]	Average temperature derivative of shear and bulk modulus ($\times 10^{-4}$ K^{-1})
r_{site}	0.072[e]	0.105	"Ideal" cation radius (nm)
r_0	0.212[f]	0.250	Avg. M-O (olivine) and M2-O (cpx) distance (nm)

Parameter	Os	Sr	Nd	Pb	Description
z	3+, 4+[h]	2+	3+	2+	Ionic charge
r_i[i]	0.063[j], 0.069	0.118	0.1098	0.119	Cation radius (nm)

[a] Data from Van Orman et al. (2001).
[b] Estimated to be similar to Fe-Mg interdiffusion coefficient (Jurewicz and Watson, 1988).
[c] Typical value for olivine (Brady, 1995).
[d] Anderson and Isaak (1995).
[e] Ionic radius of Mg^{2+} (Shannon, 1976).
[f] Brown (1980).
[g] Not used in Eqn. 10 above. The value for b of cpx is taken from Table 7 of van Orman et al. (2001).
[h] Most likely oxidation states of Os in the mantle (Borisov and Walker, 2000).
[i] Shannon (1976)
[j] Extrapolated from 4+, 5+, 6+, and 7+ radii for 6-fold coordination.

at high temperature (e.g., Joesten, 1991), though quantitative data for the elements of interest are sparse. On the other hand, grain boundary diffusion of Os may be significant because Os is strongly excluded from silicate and oxide mineral lattices (Watson, 2002). Diffusion through an interconnected interstitial melt phase could be facilitated if oxysulfide liquids have dihedral angles against silicate minerals $< 60°$ under mantle conditions (Gaetani and Grove, 1999; Rose and Brenan, 2001). However, the extreme efficiency of diffusive transport implied by such a process is not compatible with observed small-scale isotopic disequilibrium in mantle peridotite (Brandon et al., 2000; Saal et al., 2001).

Another issue specific to Os diffusion is the potential that chemical exchange can be inhibited if sulfide grains occur as inclusions sealed in other phases (Burton et al., 1999). Highly unradiogenic Os in sulfide and alloy grains from several localities (e.g., Burton et al., 1999; Alard et al., 2002; Malitch, 2002; Meibom et al., 2002) supports the hypothesis that such shielding occurs in the mantle. However, we do not think that long-term sequestration of this sort occurs in the *convecting* mantle, because new grain boundaries form continuously in the interiors of mineral grains undergoing creep associated with convection (Karato and Wu, 1993; Bystricky et al., 2000). Even if some portion of the Os in peridotite is shielded in inclusions in minerals, some sulfides in peridotite reside on grain boundaries (Burton et al., 1999; Alard et al., 2002). Because Os isotope ratios of interstitial sulfides are generally more similar to whole-rock values than those of included sulfides (Burton et al., 1999; Alard et al., 2002), shielding is not likely to be effective for Os isotope signatures in the mantle.

4.3.3. Chief Parameters Affecting Compaction

Compaction rates calculated from Eqn. 9 to 13 are influenced chiefly by matrix viscosity ($\zeta + 4/3\eta$), melt viscosity (μ) and permeability (k_ϕ). The viscosity of pyroxenite could vary considerably, depending on mineral mode, clinopyroxene composition, and temperature. We assume that pyroxenite rheology depends only on pyroxene properties, as the proportion of pyroxene in upper mantle pyroxenite is likely to be near 80% (Pertermann and Hirschmann, 2003). Whereas diopside is quite strong (Bystricky and Mackwell, 2001), the sodic pyroxene expected in recycled lithologies in the upper mantle could be very weak (Stöckhert and Renner, 1998; Jin et al., 2001). For simplicity, we assume pyroxenite matrix viscosity is 10^{18} Pa s.

The viscosity of melt also depends on melt composition and temperature. Pyroxenites produce basaltic to alkali picritic magmas at high degrees of melting (Kogiso and Hirschmann, 2001; Kogiso et al., 2001; Hirschmann et al., 2003; Pertermann and Hirschmann, 2003), and viscosities of such melts are between 1 and 10 Pa s at 1300°C (Scarfe, 1986). Here we use 1 Pa s as a representative value for μ of pyroxenite partial melt. Since partial melts from MORB-like pyroxenite are more silicic at lower degrees of melting (Pertermann and Hirschmann, 2003), μ could be much larger than 1 Pa s. However, variation in μ within several orders of magnitude does not affect the calculated results significantly.

The parameters influencing matrix permeability (n and b, Eqn. 12) depend on dihedral angle and porosity (von Bargen and Waff, 1986; McKenzie, 1989). The critical melt fraction for melt interconnection ϕ_c may also affect the permeability (Wark and Watson, 1998). We assume $n = 2$ and $b = 3000$ (McKenzie, 2000) and values for other parameters needed for Eqn. 9 to 11 are given in Table 3.

Table 3. Parameter values used in the calculations of compaction time.

Parameter	Value	Description
$\zeta + 4/3\eta$	10^{18}[a,b]	Viscosity of pyroxenite solid matrix (Pa s)
μ	1[b,c]	Viscosity of pyroxenite partial melt (Pa s)
ρ_m	3300	Density of pyroxenite solid matrix (kg/m^3)
ρ_s	2800	Density of pyroxenite partial melt (kg/m^3)
k_ϕ	$a^2\phi^2/3000$[d]	Permeability
a	0.001	Grain size (m)
g	10	Acceleration due to gravity (m/s^2)

[a] Jin et al. (2001).
[b] McKenzie (1985).
[c] Scarfe (1986).
[d] McKenzie (2000).

5. RESULTS AND DISCUSSION

5.1. Survival of Pyroxenite Signature During Partial Melting

Here we consider whether a particular pyroxenite body will compact faster than it melts and disaggregates, and then compare the rate of diffusive equilibration with surrounding peridotite relative to the faster of these two segregation processes. Figure 5 shows whether compaction or disaggregation will dominate as a function of body height (h) and melting rate. The shaded regions indicate pyroxenite melting rates appropriate for upwelling velocities ranging from that beneath a slow-spreading ridge (1 cm/yr) to beneath the center of a mantle plume (50 cm/yr). If the ratio of the compaction time to the disaggregation time is less than $1/e$ (below curve "A"), we assume that compaction is more rapid than melting and so maintains porosity close to ϕ_c. Depending on melting rate, such conditions apply to bodies with heights larger than ~1 cm to 1 m when ϕ_c is small (0.001) but to 1 to 100 m bodies for a larger ϕ_c (0.05) because the compaction length is greater for larger ϕ (McKenzie, 1985).

Having characterized the parameter space in which compaction occurs more rapidly than disaggregation, we can assess the relative rates of compaction and diffusive equilibration for bodies of different dimension. The maximum height (h) of equant bodies (i.e., $h = 2l$) that will equilibrate diffusively with surrounding peridotite for a range of $k\beta$ appear in Figure 5 as vertical lines. Figure 6 shows the effect of aspect ratio ($h/2l$) on the relative time scales of diffusive equilibration and compaction. For a given value of $k\beta$, partial melt segregates before diffusive equilibration with surrounding mantle from a pyroxenite body that plots to the right of the vertical line in Figure 5 or of the curve in Figure 6. For domain heights smaller than the compaction length (i.e., minima in $2l$ along the curves in Fig. 6), there is an inverse correlation between aspect ratio and maximum width for diffusive equilibration, that is, increases in h result in faster compaction, thereby allowing melts from narrower bodies to segregate before they equilibrate with peridotite wall-rocks. At a given value of $k\beta$, this effect amounts

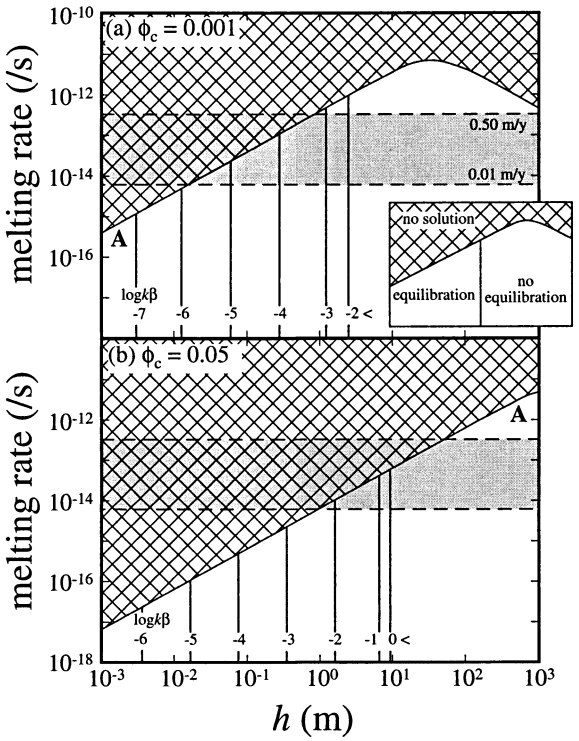

Fig. 5. Comparison between compaction time and disaggregation time for (a) $\phi_c = 0.001$ and (b) $\phi_c = 0.05$ as a function of pyroxenite body height (h). The disaggregation time is defined as that required for the porosity to increase from ϕ_c to the threshold value for disaggregation (0.4: Marsh, 1981). Below curve A, the compaction time is $1/e$ times shorter than the disaggregation time, and we assume that our constant-porosity calculations are applicable. Thin vertical lines are the maximum widths of equant bodies (aspect ratio = $h/2l = 1$) that will equilibrate diffusively with surrounding peridotite for a range of $k\beta$ values. As schematically illustrated in the inset, for a given value of $k\beta$, partial melt segregates from pyroxenite bodies before diffusive equilibration with surrounding mantle if the pyroxenite body is sufficiently wide. Shaded area represents melting rate of pyroxenite for a range of mantle upwelling rates, ranging from that of a slow-spreading ridge (0.01 m/yr) to a vigorous plume (0.5 m/yr), assuming a relatively high melt productivity, dϕ/dz, of 0.02/km (Pertermann and Hirschmann, 2003). If the pyroxenite is assumed to be somewhat more refractory, constant-porosity calculations apply to greater upwelling rates.

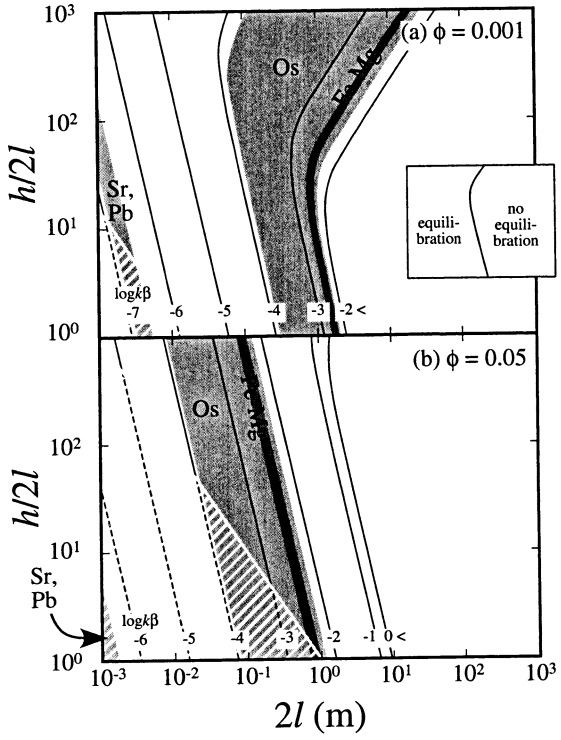

Fig. 6. Maximum sizes of partially molten bodies that will equilibrate diffusively with surrounding peridotite for a range of aspect ratios ($h/2l$). Curves give the critical body widths beyond which melt segregation by compaction is faster than diffusive equilibration at a certain value of $k\beta$ and ϕ (schematically shown in the inset). Estimated ranges of $k\beta$ for trace elements and Fe-Mg exchange are shown as shaded regions. Minima in $2l$ along the curves in panel a (out of range in panel b) occur at the compaction length (Eqn. 9; see McKenzie, 1985). Hatched parts of curves and areas indicate the region in which disaggregation is more rapid than compaction (equivalent to above curve A in Fig. 5), where our constant-porosity calculations are not applicable. This region is calculated for the case of a slow-spreading ridge melting rate of 10^{-14}/s and would be larger for a faster (plume) melting rate. A similar region also would appear at values of h higher than those shown.

to a decrease in $2l$ of about an order of magnitude for an aspect ratio of 1000 (Fig. 6b). When body heights exceed the compaction length, however, compaction times increase (McKenzie, 1985), thereby requiring wider bodies for segregation to be faster than equilibration. Such conditions apply when ϕ is small (Fig. 6a).

Thus, for large values of ϕ and an aspect ratio of 100, veins several tens of centimeters wide may expel melts with radiogenic Os. For other incompatible elements, subcentimeter-size bodies are large enough to preserve pyroxenite signatures, although it seems unlikely that our diffusion and melt segregation models give meaningful results for such small bodies. However, the calculations demonstrate that for $k\beta$ values relevant to the elements considered (Table 1) and ϕ_c on the order of 0.1 to 5%, heterogeneous domains with aspect ratios of 1 to 100 and widths of approximately a few tens of centimeters to a few meters can compact and segregate melts without diffusive equilibration of Os and incompatible tracers with peridotite matrix.

If grain-boundary diffusion in peridotite is very efficient, partially molten bodies of pyroxenite homogenize with their surrounding peridotite more rapidly and wider bodies are required for preservation of pyroxenite signatures. For example, if grain boundary transport raises D_{pd} by 2 orders of magnitude for Os, then log $k\beta$ could be as large as -1 (Table 1) and bodies nearly 10 m wide could be required to allow expulsion of radiogenic Os from pyroxenite domains (Fig. 6a). Even if it raises D_{pd} by 4 orders of magnitude (log $k\beta$ as large as 0), bodies $>$ 10 m may not be required. Thus, it is possible that radiogenic Os and other pyroxenite signatures can segregate from rather small sources and even if more rapid diffusive mechanisms are operative, the bodies could still be of relatively modest dimension.

The processes considered here may affect major element compositions of partial melts extracted from pyroxenite bodies. Based on estimates of k and β values for Fe-Mg exchange

between pyroxenite melt and peridotite (Table 1), pyroxenite bodies 0.1 to 10 m wide will expel partial melts with original Fe/Mg ratios for ϕ of 0.001 to 0.05 (Fig. 6). Interestingly, for a considerable range of parameters (porosity, aspect ratio), there is an intermediate-size pyroxenite body (tens of centimeters to meters) that will equilibrate with peridotite with respect to Mg#, but not for incompatible tracers (Sr, Nd, Pb) and possibly not for Os isotopes if the $k\beta$ value for Os is at the lower ends of our estimates (Fig. 6). Such bodies could produce high Mg# partial melts with enriched mantle signatures.

Thus, differing transport properties and distributions of various chemical tracers can result in decoupling of elemental and isotopic signatures during partial melting. Bodies greater than several meters thick may retain all of the signature of their original source and bodies of centimeter size can retain signatures of slow-diffusing tracers, such as Sr isotopes, but lose others, such as Mg#.

A key point is that correlations between tracers in magmatic suites, such as those illustrated in Figure 2, imply that these tracers are *not* diffusively decoupled. Thus, a component with radiogenic Os, Sr, and Pb would presumably derive from bodies large enough to prevent equilibration of Os, which is the faster-diffusing element. With sufficiently precise constraints on the relative diffusivities of components, the presence or absence of correlations of components with differing diffusivities may provide improved constraints on the dimensions of heterogeneous bodies. For example, an absence of correlations between Os isotopes and Fe/Mg ratios may imply that bodies are intermediate in dimension between the equilibration lengths of these two tracers.

5.2. Survival of Heterogeneous Bodies Before Melting

Here we return to the question of the size of bodies that will retain distinct geochemical signatures in the solid state during extended residence in the mantle, as these are the minimum dimensions of heterogeneities that can be delivered to basalt source regions. Diffusion time scales for solid pyroxenite domains can be calculated using Eqn. 2 to 6, with $\phi = 0$ if k in Eqn. 5 is replaced by $k_{solid} = c_{pd}/c_{xs}$. Consequently, T_d in Eqn. 7 is calculated in which ϕ is the fraction of pyroxenite solid (i.e., $\phi = 1$), $\beta = \beta_{solid} = (D_{pd}/D_{xs})^{0.5}$ and $T = tD_{xs}/l^2$. Estimated values of k_{solid} and β_{solid} are listed in Table 4. The wide range of possible temperatures and pressures experienced by a pyroxenite domain during extended residence in the mantle makes it difficult to estimate the vigor of diffusive exchange with surrounding peridotite, so we apply diffusivities estimated for 1300°C, the same as for the partially molten case. Diffusion of Os in clinopyroxene is estimated using the model of Van Orman et al. (2001), and those of other elements are taken from the literature (Table 4). Then D_{xs} values are calculated taking into account the effect of K_{cpx}, the partition coefficient between host mineral and clinopyroxene; i.e., $D_{xs} = D_{cpx}/K_{cpx}$. Values for k_{solid} are calculated from peridotite-basalt and clinopyroxene-basalt partition coefficients (Table 4).

The resulting calculated equilibration lengths for 10^9 yr of residence are plotted against D_{xs} in Figure 7. Length scales of diffusive equilibration vary according to the applicable values of k_{solid} and β_{solid} for each element. All of the original signatures survive 10^9 yr of residence in the mantle for bodies larger than a few meters. Comparison of Figures 6 and 7 shows that for a given element, bodies that are affected by solid-state diffusion in 10^9 yr are similar in width or larger than those that are affected during melting and segregation. Thus, pyroxenite bodies large enough to remain compositionally distinct for 10^9 yr in the mantle can segregate partial melts faster than diffusive equilibration with surrounding mantle.

Table 4. Estimated parameters for subsolidus diffusion between pyroxenite and peridotite.

Element	log D_{cpx}	log K_{cpx}[a]	log D_{xs}[b]	log k_{solid}[c]	log β_{solid}
Os	–14.7 to –12.6[d]	4 to 5[e]	–19.7 to –16.6	1.5 to 2.5	–1.9 to –0.9
Sr	–17.9[f]	0	–17.9	–0.8	–1.1
Nd	–19.4[g]	0	–19.4	–0.8	–2.9
Pb	–16.8[h]	0	–16.8	–0.8	–0.7
Fe-Mg	–17.5[i]	0	–17.5	0	1.6

[a] Partition coefficient between host mineral and clinopyroxene.
[b] = log (D_{cpx}/K_{cpx}).
[c] Data sources are as in Table 1.
[d] Calculated using the model of Van Orman et al. (2001) with parameters listed in Table 2.
[e] Assumed to be same as the value for K (Table 1).
[f] Sneeringer et al. (1984).
[g] Van Orman et al. (2001).
[h] Cherniak (2001).
[i] Dimanov and Sautter (2000).

5.3. Fate of Melts Expelled From Pyroxenite Domains

Efficient segregation of partial melts from pyroxenite does not guarantee that the liquids will survive passage through overlying peridotite. A key point is that pyroxenite heterogeneities cannot be the principal source of radiogenic Os in

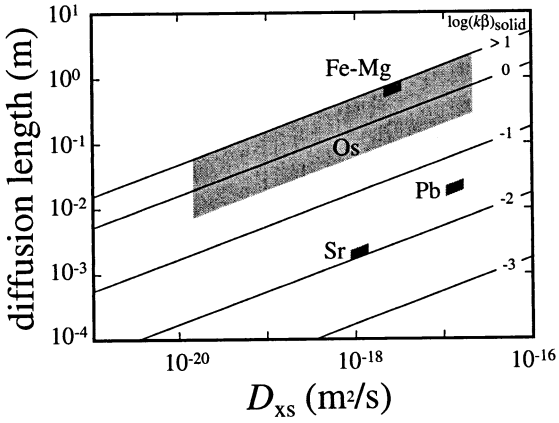

Fig. 7. Diffusion lengths for solid pyroxenite bodies interacting with surrounding peridotite, plotted against diffusion coefficient of pyroxenite (D_{xs}) for 10^9 yr of residence in the mantle. Elements are shown in shaded fields according to their estimated ranges of D_{xs} and $(k\beta)_{solid}$. In all case, solid-state diffusion is only effective in bodies less than several meters wide over this time interval, but the Fe/Mg ratios are affected for larger bodies than Pb and Sr isotope ratios, and possibly than Os isotope ratios if the $(k\beta)_{solid}$ or D_{xs} value for Os is at the lower ends of our estimates. We argue that for exchange between subsolidus bodies, pyroxenites that have had their Fe/Mg ratios altered by exchange with peridotite can retain exotic isotope signatures owing to differences in D_{xs}.

basalts unless their partial melts escape extensive interaction with peridotite before mixing with peridotite-derived melt. Because the upper mantle appears to be dominated by peridotite rich in unradiogenic Os (Fig. 1) (Shirey and Walker, 1998; Meibom et al., 2002), this constraint also applies to any plausible source of radiogenic Os, provided that the length scale of the radiogenic source is small compared to the transport distance between the source and the surface. Major element signatures of the pyroxenite source could also be destroyed (Yaxley and Green, 1998), though incompatible trace element signatures may not (Hauri, 1997).

Two processes that may aid transport of melt with pyroxenite signatures through peridotitic mantle are time-dependent segregation into fractures or other melt-rich bands, as described in section 3.2, or formation of high melt/rock ratio conduits, leading to dunite channels (Kelemen et al., 1997; Lundstrom et al., 2000). Radiogenic Os in dunites may be evidence of the latter (Burton et al., 2000; Becker et al., 2001). Interestingly, pyroxenite sources may aid in both processes, as melt-rich regions in the pyroxenite may nucleate segregations (section 3.2) or aid formation of dunites (Lundstrom et al., 2000).

5.4. Comment on Yaxley and Green (1998)

Yaxley and Green (1998) showed that partial melts of quartz eclogite freeze when allowed to react with peridotite. In their view, this freezing-in may fertilize upwelling peridotite just before it begins to partially melt. The resulting peridotite would melt at shallower depths according to phase relations little-different from typical mantle lherzolite, but with trace element and isotopic enrichments reflecting the pyroxenite contribution. Although this scenario may be accurate in some cases, it has three potential shortcomings. First, it cannot explain radiogenic Os in oceanic basalts, as the Os budget of mantle fertilized in this way will be dominated by the original peridotite (i.e., having unradiogenic Os). Second, it is applicable to pyroxenites that generate silicic liquids but not to nepheline-normative partial melts expected from silica-deficient pyroxenites (Hirschmann et al., 2003). Third, a freezing reaction between silicic partial melts and peridotite will create a permeability barrier (section 3.2), thereby trapping melt in peridotite/pyroxenite reaction zones and preventing pervasive refertilisation of peridotite by this mechanism. Such zones would presumably become overwhelmed with pyroxenite-derived melt, leading to enriched domains with phase equilibria characteristics unlike normal peridotite.

6. SUMMARY AND CONCLUDING REMARKS

The radiogenic Os component in OIB may be derived from pyroxenite domains, so long as mixing between these sources and non-radiogenic peridotitic Os is between partial melts. Our analysis shows that pyroxenite bodies submeter to a few meter wide can retain and produce melts with distinctive geochemical signatures under typical mantle melting conditions. These dimensions are similar to those observed in lithospheric mantle samples and those expected to result from approximately billion-year convective stretching of subducted crust. We argue that this model presents the most satisfactory explanation for the Os isotope systematics of OIB at the present time, but we recognize that transport through overlying peridotite remains a significant problem.

We affirm the conclusion of Hofmann and Hart (1978) that solid state diffusion has limited effect on mantle heterogeneities in the shallow mantle, though much remains to be learned regarding diffusivities in deep mantle environments. In general, diffusive interaction with peridotite should cause significant Mg# increases in pyroxenite over length scales larger than for most other tracers. Therefore, enriched components in high Mg# lavas (e.g., Norman and Garcia, 1999; Niu and O'Hara, 2003) may not be strong evidence against pyroxenite sources.

Finally, the style of melting and the dynamics of melt transport associated with pyroxenite sources depend on the size of the pyroxenite bodies. Small (centimeter-sized) heterogeneous domains may not contribute significant radiogenic Os to basalts, but if sufficiently abundant they may have measurable effects on incompatible isotopes (Sr, Nd, Pb) and trace elements. Larger domains can potentially also affect Os isotope ratios of basalts. Assuming that radiogenic Os in basalts derives from pyroxenite, observed correlations between radiogenic Os and incompatible tracers (Fig. 2) suggest that dimensions of typical pyroxenite bodies in basalt source regions are large enough to allow preservation of radiogenic Os isotope signatures.

Acknowledgments—We gratefully acknowledge Shun Karato, Eiichi Takahashi, David Kohlstedt, Daisuke Yamazaki, Ken Koga, Ritsuo Morishita, and Ben Holtzmann for assistance and for stimulating discussions, and Glenn Gaetani and Harry Becker for their comments. We also thank constructive reviews by Stan Hart, John Lassiter, Jim van Orman, and Fred Frey. This work was supported by NSF 9876255.

Associate editor: F. A. Frey

REFERENCES

Alard O., Griffin W. L., Pearson N. J., Lorand J.-P., and O'Reilly S. Y. (2002) New insights into the Re-Os systematics of sub-continental lithospheric mantle from in situ analysis of sulphides. *Earth Planet. Sci. Lett.* **203,** 651–663.

Allègre C. and Turcotte D. L. (1986) Implications of a two-component marble-cake mantle. *Nature* **323,** 123–127.

Anderson O. L. and Isaak D. G. (1995) Elastic constants of mantle minerals at high temperature. In *Mineral Physics and Crystallography: A Handbook of Physical Constants*, AGU Reference Shelf 2 (ed. T. J. Aherns), pp. 64–97. American Geophysical Union, Washington, DC.

Beattie P. (1993) The generation of uranium series disequilibria by partial melting of spinel peridotite: Constraints from partitioning studies. *Earth Planet. Sci. Lett.* **117,** 379–391.

Beattie P. (1994) Systematics and energetics of trace-element partitioning between olivine and silicate melts: Implications for the nature of mineral/melt partitioning. *Chem. Geol.* **117,** 57–71.

Becker H. (2000) Re-Os fractionation in eclogites and blueschists and the implications for recycling of oceanic crust into the mantle. *Earth Planet. Sci. Lett.* **177,** 287–300.

Becker H., Shirey S. B., and Carlson R. W. (2001) Effects of melt percolation on the Re-Os systematics of peridotites from a Paleozoic convergent plate margin. *Earth Planet. Sci. Lett.* **188,** 107–121.

Bennet V. C., Norman M. D., and Garcia M. O. (2000) Rhenium and platinum group element abundances correlated with mantle source components in Hawaiian picrites: Sulphides in the plume. *Earth Planet. Sci. Lett.* **183,** 513–526.

Blichert-Toft J., Albarède F., and Kornprobst J. (1999) Lu-Hf isotope systematics of garnet pyroxenites from Beni–Bousera, Morocco: Implications for basalt origin. *Science* **283,** 1303–1306.

Blusztajn J., Hart S. R., Ravizza G., and Dick H. J. B. (2000) Platinum-group elements and Os isotopic characteristics of the lower oceanic crust. *Chem. Geol.* **168,** 113–122.

Bodinier J. L., Guiraud M., Fabriés J., Dostal J., and Dupuy C. (1987) Petrogenesis of layered pyroxenites from the Lherz, Freychinède and Prades ultramafic bodies (Ariège, French Pyrénées). *Geochim. Cosmochim. Acta* **51,** 279–290.

Borisov A. and Walker R. J. (2000) Os solubility in silicate melts: New efforts and results. *Am. Mineral.* **85,** 912–917.

Brady J. B. (1995) Diffusion data for silicate minerals, glasses, and liquids. In *Mineral Physics and Crystallography: A Handbook of Physical Constants*, AGU Rererence Shelf 2 (ed. T. J. Ahrens), pp. 269–290. American Geophysical Union, Washington, DC.

Brandon A. D., Walker R. J., Morgan J. W., Norman M. D., and Prichard H. M. (1998) Coupled ^{186}Os and ^{187}Os evidence for core-mantle interaction. *Science* **280,** 1570–1573.

Brandon A. D., Norman M. D., Walker R. J., and Morgan J. W. (1999) ^{186}Os-^{187}Os systematics of Hawaiian picrites. *Earth Planet. Sci. Lett.* **174,** 25–42.

Brandon A. D., Snow J. E., Walker R. J., Morgan J. W., and Mock T. D. (2000) ^{190}Pt-^{186}Os and ^{187}Re-^{187}Os systematics of abyssal peridotites. *Earth Planet. Sci. Lett.* **177,** 319–335.

Brown G. E. (1980) Olivines and silicate spinels. *Rev. Mineral.* **5,** 275–381.

Büchl A., Brügmann G., Batanova V. G., Münker C., and Hofmann A. W. (2002) Melt percolation monitored by Os isotopes and HSE abundances: A case study from the mantle section of the Troodos Ophiolite. *Earth Planet. Sci. Lett.* **204,** 385–402.

Bulatov V. K., Girnis A. V., and Brey G. P. (2002) Experimental melting of a modally heterogeneous mantle. *Mineral. Petrol.* **75,** 131–152.

Burton K. W., Schiano P., Birck J. L., and Allegre C. J. (1999) Osmium isotope disequilibrium between mantle minerals in a spinel-lherzolite. *Earth Planet. Sci. Lett.* **172,** 311–322.

Burton K. W., Schiano P., Birck J. L., Allegre C. J., Rehkamper M., Halliday A. N., and Dawson J. B. (2000) The distribution and behaviour of rhenium and osmium amongst mantle minerals and the age of the lithospheric mantle beneath Tanzania. *Earth Planet. Sci. Lett.* **183,** 93–106.

Bystricky M. and Mackwell S. (2001) Creep of dry clinopyroxene aggregates. *J. Geophys. Res.* **106,** 13443–13454.

Bystricky M., Kunze K., Burlini L., and Burg J. P. (2000) High shear strain of olivine aggregates: Rheological and seismic consequences. *Science* **290,** 1564–1567.

Carlson R. W. and Irving A. J. (1994) Depletion and enrichment history of subcontinental lithospheric mantle: An Os, Sr, Nd and Pb isotopic study of ultramafic xenoliths from the northwestern Wyoming Craton. *Earth Planet. Scie. Lett.* **126,** 457–472.

Carlson R. W, Nowell G. M (2001) Olivine-poor sources for mantle-derived magmas: Os and Hf isotopic evidence from potassic magmas of the Colorado Plateau. *Geochem. Geophys. Geosys.* **2,** 2000.GC000128.

Chen C.-Y. and Frey F. A. (1985) Trace element and isotopic geochemistry of lavas from Haleakala Volcano, East Maui, Hawaii: Implications for the origin of Hawaiian basalts. *J. Geophys. Res.* **90,** 8743–8768.

Cherniak D. J (2001) Pb diffusion in Cr diopside, augite, and enstatite, and consideration of the dependence of cation diffusion in pyroxene on oxygen fugacity. *Chem. Geol.* **177**.

Class C. and Goldstein S. L. (1997) Plume-lithosphere interactions in the ocean basins: Constraints from the source mineralogy. *Earth Planet. Sci. Lett.* **150,** 245–260.

Crank J. (1956) The Mathematics of Diffusion. Oxford University Press, New York.

Daines M. J. and Kohlstedt D. L. (1993) A laboratory study of melt migration. *Philos. Trans. R. Soc. London, Ser. A* **342,** 43–52.

Dimanov A. and Sautter V. (2000) "Average" interdiffusion of (Fe, Mn)-Mg in natural diopside. *Eur. J. Mineral.* **12,** 749–760.

Esperanca S., Carlson R. W., Shirey S. B., and Smith D. (1997) Dating crust-mantle separation: Re-Os isotopic study of mafic xenoliths from central Arizona. *Geology* **25,** 651–654.

Fisler D. K., Mackwell S. J., and Petsch S. (1997) Grain boundary diffusion in enstatite. *Phys. Chem. Miner.* **24,** 264–273.

Gaetani G. A. and Grove T. L. (1999) Wetting of mantle olivine by sulfide melt: Implications for Re/Os ratios in mantle peridotite and late-stage core formation. *Earth Planet. Sci. Lett.* **169,** 147–163.

Gast P. W., Tilton G. R., and Hedge C. (1964) Isotopic composition of lead and strontium from Ascension and Gough Islands. *Science* **145,** 1181–1185.

Hanyu T. and Kaneoka I. (1997) The uniform and low ^{3}He/^{4}He ratios of HIMU basalts as evidence for their origin as recycled materials. *Nature* **290,** 273–276.

Hart S. R. and Dunn T. (1993) Experimental cpx/melt partitioning of 24 trace elements. *Contrib. Mineral. Petrol.* **113,** 1–8.

Hart S. R. and Ravizza G. (1996) Os partitioning between phases in lherzolite and basalt. In *Earth Processes: Reading the Isotopic Code*, Geophysical Monograph 95 (eds. S. R. Hart and A. Basu), pp. 123–134. American Geophysical Union, Washington, DC.

Hauri E. H. (1996) Major-element variability in the Hawaiian mantle plume. *Nature* **382,** 415–419.

Hauri E. H. (1997) Melt migration and mantle chromatography, 1: Simplified theory and conditions for chemical and isotopic decoupling. *Earth Planet. Sci. Lett.* **153,** 1–19.

Hauri E. H. and Hart S. R. (1993) Re-Os isotope systematics of HIMU and EMII oceanic island basalts from the south Pacific Ocean. *Earth Planet. Sci. Lett.* **114,** 353–371.

Hauri E. H. and Kurz M. D. (1997) Melt migration and mantle chromatography, 2: A time-series Os isotope study of Mauna Loa volcano, Hawaii. *Earth Planet. Sci. Lett.* **153,** 21–36.

Hauri E. H., Wagner T. P., and Grove T. L. (1994) Experimental and natural partitioning of Th, U, Pb and other trace elements between garnet, clinopyroxene and basaltic melts. *Chem. Geol.* **117,** 149–166.

Hauri E. H., Lassiter J. C., and DePaolo D. J. (1996) Osmium isotope systematics of drilled lavas from Mauna Loa, Hawaii. *J. Geophys. Res.* **101,** 11793–77806.

Hirschmann M. M. and Stolper E. M. (1996) A possible role for garnet pyroxenite in the origin of the "garnet signature" in MORB. *Contrib. Mineral. Petrol.* **124,** 185–208.

Hirschmann M. M., Kogiso T., Baker M. B., and Stolper E. M. (2003) Alkalic magmas generated by partial melting of garnet pyroxenite. *Geology* **31,** 481–484.

Hofmann A. W. (1980) Diffusion in natural silicate melts: A critical review. In *Physics of Magmatic Processes* (ed. R. B. Hargraves), pp. 385–417. Princeton University Press, Princeton, NJ.

Hofmann A. W. and Hart S. R. (1978) An assessment of local and regional isotopic equilibrium in the mantle. *Earth Planet. Sci. Lett.* **38,** 44–62.

Ishii M. and Tromp J. (1999) Normal-mode and free-air gravity constraints on lateral variations in velocity and density of Earth's mantle. *Science* **285,** 1231–1236.

Iwamori H. (1993) A model for disequilibrium mantle melting incorporating melt transport by porous and channel flows. *Nature* **366,** 734–737.

Jin Z. M., Zhang J., Green H. W., and Jin S. (2001) Eclogite rheology: Implications for subducted lithosphere. *Geology* **29,** 667–670.

Joesten R. (1991) Grain-boundary diffusion kinetics in silicate and oxide minerals: Selected topics in geochemistry. In *Diffusion, Atomic Ordering, and Mass Transport* (ed. J. Ganguly), pp. 345–395. Springer-Verlag, New York.

Jurewicz A. J. G. and Watson E. B. (1988) Cations in olivine, part 2: Diffusion in olivine xenocrysts, with applications to petrology and mineral physics. *Contrib. Mineral. Petrol.* **99,** 186–201.

Kamber B. S. and Collerson K. D. (1999) Origin of ocean-island basalts: A new model based on lead and helium isotope systematics. *J. Geophys. Res.* **104,** 25479–25491.

Kamber B. S. and Collerson K. D. (2000) Role of "hidden" deeply subducted slabs in mantle depletion. *Chem. Geol.* **166,** 241–254.

Kaneshima S. and Helffrich G. (1999) Dipping low-velocity later in the mid-lower mantle: Evidence for geochemical heterogeneity. *Science* **283,** 1888–1891.

Karato S. and Wu P. (1993) Rheology of the upper mantle—A synthesis. *Science* **260,** 771–778.

Kelemen P. B., Hirth G., Shimizu N., Spiegelman M., and Dick H. J. B. (1997) A review of melt migration processes in the adiabatically

upwelling mantle beneath oceanic spreading ridges. *Philos. Trans. R. Soc. London, Ser. A* **355,** 283–318.
Kellogg L. H. and Turcotte D. L. (1990) Mixing and the distribution of heterogeneities in a chaotically convecting mantle. *J. Geophys. Res.* **95,** 421–432.
Kogiso T. and Hirschmann M. M. (2001) Experimental study of clinopyroxenite partial melting and the origin of ultra-calcic melt inclusions. *Contrib. Mineral. Petrol.* **142,** 347–360.
Kogiso T., Tatsumi Y., and Nakano S. (1997) Trace element transport during dehydration processes in the subducted oceanic crust: 1. Experiments and implications for the origin of ocean island basalts. *Earth Planet. Sci. Lett.* **148,** 193–205.
Kogiso T., Hirschmann M. M., and Frost D. J. (2001) Partial melting experiments of Mg-rich garnet clinopyroxenite and the origin of HIMU basalts. *Eos. Trans. Am. Geophys. Union* **82,** S429.
Kress V. C. and Ghiorso M. S. (1995) Multicomponent diffusion in basaltic melts. *Geochim. Cosmochim. Acta* **59,** 313–324.
Kumar N., Reisberg L., and Zindler A. (1996) A major and trace element and strontium, neodymium, and osmium isotopic study of a thick pyroxenite layer from the Beni Bousera Ultramafic Complex of northern Morocco. *Geochim. Cosmochim. Acta* **60,** 1429–1444.
Kushiro I., Syono Y., and Akimoto S. (1968) Melting of a peridotite nodule at high pressures and high water pressures. *J. Geophys. Res.* **73,** 6023–6029.
Lassiter J. C., Hauri E. H., Reiners P. W., and Garcia M. O. (2000) Generation of Hawaiian post-erosional lavas by melting of a mixed lherzolite/pyroxenite source. *Earth Planet. Sci. Lett.* **178,** 269–284.
Lee C.-T. (2002) Platinum-group element geochemistry of peridotite xenoliths from the Sierra Nevada and the Basin and Range, California. *Geochim. Cosmochim. Acta* **66,** 3987–4005.
Lundstrom C. C. (2000) Rapid diffusive infiltration of sodium into partially molten peridotite. *Nature* **403,** 527–530.
Lundstrom C. C., Gill J., and Williams Q. (2000) A geochemically consistent hypothesis for MORB generation. *Chem. Geol.* **162,** 105–126.
Maclennan J., Jull M., McKenzie D., Slater L., and Grönvold K. (2002) The link between volcanism and deglaciation in Iceland. *Geochem. Geophys. Geosys.* **5,** 10.1029/2001GC000282.
Malitch K. N. (2002) Constraints on melting and osmium isotopic sources in the ophiolitic upper mantle: Evidence from Ru-Os sulfides and Os- Ir-Ru alloys. *Geochim. Cosmochim. Acta* **66,** A478–A478.
Marcantonio F., Zindler A., Elliott T., and Staudigel H. (1995) Os isotope systematics of La Parma, Canary Islands: Evidence for recycled crust in the mantle source of HIMU ocean islands. *Earth Planet. Sci. Lett.* **133,** 397–410.
Marsh B. D. (1981) On the crystallinity, probability of occurrence, and rheology of lava and magma. *Contrib. Mineral. Petrol.* **78,** 85–98.
Martin C. E., Carlson R. W., Shirey S. B., Frey F. A., and Chen C.-Y. (1994) Os isotopic variation in basalts from Haleakala Volcano, Maui, Hawaii; a record of magmatic processes in oceanic mantle and crust. *Earth Planet. Sci. Lett.* **128,** 287–301.
McBride J. S., Lambert D. D., Greig A., and Nicholls I. A. (1996) Multistage evolution of Australian subcontinental mantle: Re-Os isotopic constraints from Victorian mantle xenoliths. *Geology* **24,** 631–634.
McCulloch M. T. and Gamble J. A. (1991) Geochemical and geodynamical constraints on subduction zone magmatism. *Earth Planet. Sci. Lett.* **102,** 358–374.
McKay G. A. (1986) Crystal/liquid partitioning of REE in basaltic systems: Extreme fractionation of REE in olivine. *Geochim. Cosmochim. Acta* **50,** 69–79.
McKenzie D. (1984) The generation and compaction of partially molten rock. *J. Petrol.* **25,** 713–765.
McKenzie D. (1985) The extraction of magma from the crust and mantle. *Earth Planet. Sci. Lett.* **74,** 81–91.
McKenzie D. (1989) Some remarks on the movement of small melt fractions in the mantle. *Earth Planet. Sci. Lett.* **95,** 53–72.
McKenzie D. (2000) Constraints on melt generation and transport from U-series activity ratios. *Chem. Geol.* **162,** 81–94.
Meibom A., Sleep N. H., Chamberlain C. P., Coleman R. G., Frei R., Hren M. T., and Wooden J. L. (2002) Re-Os isotopic evidence for long-lived heterogeneity and equilibration processes in the Earth's upper mantle. *Nature* **419,** 705–708.
Merveilleux du Vignaux N. and Fleitout L. (2001) Stretching and mixing of viscous blobs in Earth's mantle. *J. Geophys. Res.* **106,** 30893–30908.
Milke R., Wiedenbeck M., and Heinrich W. (2001) Grain boundary diffusion of Si, Mg, and O in enstatite reaction rims: A SIMS study using isotopically doped reactants. *Contrib. Mineral. Petrol.* **142,** 15–26.
Niu Y, O'Hara M. J (2003) Origin of ocean island basalts: A new perspective from petrology, geochemistry, and mineral physics considerations. *J. Geophys. Res.* **108,** 10.1029/2002JB002048.
Norman M. D. and Garcia M. O. (1999) Primitive magmas and source characteristics of the Hawaiian plume: Petrology and geochemistry of shield picrites. *Earth Planet. Sci. Lett.* **168,** 27–44.
Olive V., Ellam R. M., and Harte B. (1997) A Re-Os isotope study of ultramafic xenoliths from the Matsoku kimberlite. *Earth Planet. Sci. Lett.* **150,** 129–140.
Pearson D. G., Shirey S. B., Carlson R. W., Boyd F. R., Pokhilenko N. P., and Shimizu N. (1995) Re-Os, Sm-Nd, and Rb-Sr isotope evidence for thick Archaean lithospheric mantle beneath the Silurian craton modified by multistage metasomatism. *Geochim. Cosmochim. Acta* **59,** 959–977.
Pertermann M. and Hirschmann M. M. (2003) Partial melting experiments on a MORB-like pyroxenite between 2 and 3 GPa: Constraints on the presence of pyroxenites in basalt source regions from solidus location and melting rate. *J. Geophys. Res.* **108,** 2125.
Phipps Morgan J. (1999) Isotope topography of individual hotspot basalt arrays: Mixing curves or melt extraction trajectories? *Geochem. Geophys. Geosys.* **1,** 1999.GC000004.
Putirka K. (1999) Clinopyroxene + liquid equilibria to 100 kbar and 2450 K. *Contrib. Mineral. Petrol.* **135,** 151–163.
Ravizza G., Blusztajn J., and Prichard H. M. (2001) Re-Os systematics and platinum-group element distribution in metalliferous sediments from the Troodos ophiolite. *Earth Planet. Sci. Lett.* **188,** 369–381.
Reiners P. W. (1998) Reactive melt transport in the mantle and geochemical signatures of mantle-derived magmas. *J. Petrol.* **39,** 1039–1061.
Reiners P. W (2002) Temporal-compositional trends in intraplate basalt eruptions: Implications for mantle heterogeneity and melting processes. *Geochem. Geophys. Geosys.* **3,** 10.1029/2001GC000250.
Reisberg L., Allègre C. J., and Luck J.-M. (1991) The Re-Os systematics of the Ronda Ultramafic Complex of southern Spain. *Earth Planet. Sci. Lett.* **105,** 196–213.
Reisberg L., Zindler A., Marcantonio F., White W., Wyman D., and Weaver B. (1993) Os isotope systematics in ocean island basalts. *Earth Planet. Sci. Lett.* **120,** 149–167.
Riley G. N. J., Kohlstedt D. L., and Richter F. M. (1990) Melt migration in a silicate liquid-olivine system: An experimental test of compaction theory. *Geophys. Res. Lett.* **17,** 2101–2104.
Roeder P. L. and Emslie R. F. (1970) Olivine-liquid equilibrium. *Contrib. Mineral. Petrol.* **29,** 275–289.
Rose L. A. and Brenan J. M. (2001) Wetting properties of Fe-Ni-Co-Cu-O-S melts against olivine: Implications for sulfide melt mobility. *Econ. Geol. Bull. Soc. Econ. Geol.* **96,** 145–157.
Roy-Barman M., Luck J. M., and Allègre C. J. (1996) Os isotopes in orogenic lherzolite massifs and mantle heterogeneities. *Chem. Geol.* **130,** 55–64.
Rudnick R. L., Barth M., Horn I., and McDonough W. F. (2000) Rutile-bearing refractory eclogites: Missing link between continents and depleted mantle. *Science* **287,** 278–281.
Saal A. E., Hart S. R., Shimizu N., Hauri E. H., and Layne G. D. (1998) Pb isotopic variability in melt inclusions from oceanic island basalts, Polynesia. *Science* **282,** 1481–1484.
Saal A. E., Hart S. R., Takazawa E., Frey F. A., and Shimizu N. (2001) Re-Os isotopes in the Horoman peridotite: Evidence for refertilization? *J. Petrol.* **42,** 25–37.
Salters V. J. M. and Dick H. J. B. (2002) Mineralogy of the mid-ocean-ridge basalt source from neodymium isotopic composition of abyssal peridotites. *Nature* **418,** 68–72.
Scarfe C. M. (1986) Viscosity and density of silicate melts. In *Silicate Melts: Their Properties and Structure Applied to Problems in Geochemistry, Petrology, Economic Geology and Planetary Geology* (ed. C. M. Scarfe), pp. 36–56. Mineralogical Association of Canada.

Schiano P., Brick J.-L., and Allegre C. J. (1997) Osmium-strontium-neodymium-lead isotopic covariations in mid-ocean ridge basalt glasses and the heterogeneity of the upper mantle. *Earth Planet. Sci. Lett.* **150,** 363–379.

Schiano P., Burton K. W., Dupre B., Birck J. L., Guille G., and Allegre C. J. (2001) Correlated Os-Pb-Nd-Sr isotopes in the Austral-Cook chain basalts: The nature of mantle components in plume sources. *Earth Planet. Sci. Lett.* **186,** 527–537.

Shannon R. D. (1976) Revised effective ionic radii and systematic studies of interatomic distances in halides and chalcogenides. *Acta Cryst.* **A32,** 751–767.

Shirey S. B. and Walker R. J. (1998) The Re-Os isotope system in cosmochemistry and high-temperature geochemistry. *Ann. Rev. Earth Planet. Sci.* **26,** 423–500.

Sneeringer M., Hart S. R., and Shimizu N. (1984) Strontium and samarium diffusion in diopside. *Geochim. Cosmochim. Acta* **48,** 1589–1608.

Sobolev A. V., Hofmann A. W., and Nikogosian I. K. (2000) Recycled oceanic crust observed in "ghost plagioclase" with the source of Mauna Loa Lavas. *Nature* **404,** 986–990.

Spiegelman M. and Kenyon P. (1992) The requirements for chemical disequilibrium during magma migration. *Earth Planet. Sci. Lett.* **109,** 611–620.

Stevenson D. J. (1989) Spontaneous small-scale melt segregation in partial melts undergoing deformation. *Geophys. Res. Lett.* **16,** 1067–1070.

Stöckhert B. and Renner J. (1998) Rheology of crustal rocks at ultra-high pressure. In *When Continents Collide: Geodynamics and Geochemistry of Ultrahigh-Pressure Rocks* (eds. B. R. Hacker and J. G. Liou), pp. 57–95. Kluwer.

Takahashi E. and Nakajima K. (2002) Melting process in the Hawaiian plume: An experimental study. In *Hawaiian Volcanoes: Deep Underwater Perspectives*, Geophysical Monograph 128 (eds. E. Takahashi, P. W. Lipman, M. Garcia, J. Naka, and S. Aramaki), pp. 403–418. American Geophysical Union, Washington, DC.

Toramaru A. and Fujii N. (1986) Connectivity of melt phase in a partially molten peridotite. *J. Geophys. Res.* **91,** 9239–9252.

van Keken P. and Zhong S. J. (1999) Mixing in a 3D spherical model of present-day mantle convection. *Earth Planet. Sci. Lett.* **171,** 533–547.

van Orman J. A., Grove T. L., and Shimizu N. (2001) Rare earth element diffusion in diopside: influence of temperature, pressure, and ionic radius, and an elastic model for diffusion in silicates. *Contrib. Mineral. Petrol.* **141,** 687–703.

von Bargen N. and Waff H. S. (1986) Permeabilities, interfacial areas and curvatures of partially molten systems: Results of numerical computations of equilibrium microstructures. *J. Geophys. Res.* **91,** 9261–9276.

Walker R. J., Morgan J. W., and Horan M. F. (1995) ^{187}Os enrichment in some plumes: evidence for core-mantle interaction? *Science* **269,** 819–822.

Walker R. J., Storey M., Kerr A. C., Tarney J., and Arndt N. T. (1999) Implications of ^{187}Os isotopic heterogeneities in a mantle plume: Evidence from Gorgona Island and Curacao. *Geochim. Cosmochim. Acta* **63,** 713–728.

Wark D. A. and Watson E. B. (1998) Grain-scale permeabilities of texturally equilibrated, monomineralic rocks. *Earth Planet. Sci. Lett.* **164,** 591–605.

Watson B (2002) Mobility of siderophile elements in grain boundaries of periclase and periclace/olivine aggregates. *Eos: Trans. Am. Geophys. Union* **83,** Spring Meet. Suppl., Abstract V52B-03.

Widom E., Hoernle K. A., Shirey S. B., and Schmincke H.-U. (1999) Os isotope systematics in the Canary Islands and Madeira: Lithospheric contamination and mantle plume signatures. *J. Petrol.* **40,** 279–296.

Yamazaki D., Kato T., Yurimoto H., Ohtani E., and Toriumi M. (2000) Silicon self-diffusion in $MgSiO_3$ perovskite at 25 GPa. *Phys. Earth Planet. Inter.* **119,** 299–309.

Yasuda A., Fujii T., and Kurita K. (1994) Melting phase relations of an anhydrous mid-ocean ridge basalt from 3 to 20 GPa: Implications for the behavior of subducted oceanic crust in the mantle. *J. Geophys. Res.* **99,** 9401–9414.

Yaxley G. M. and Green D. H. (1998) Reactions between eclogite and peridotite: Mantle refertilisation by subduction of oceanic crust. *Schweiz. Mineral. Petrogr. Mitt.* **78,** 243–255.

Yund R. A. (1997) Rates of grain boundary diffusion through enstatite and forsterite reaction rims. *Contrib. Mineral. Petrol.* **126,** 224–236.

Zhao D. (2001) Seismic structure and origin of hotspots and mantle plumes. *Earth Planet. Sci. Lett.* **192,** 251–265.

Zindler A. and Hart S. (1986) Chemical geodynamics. *Ann. Rev. Earth Planet. Sci.* **14,** 493–571.